IET Nanobiotechnology

Research Article

IET Journals
The Institution of Engineering and Technology

Magnetic soy protein isolate–bovine serum albumin nanoparticles preparation as a carrier for inulinase immobilisation

ISSN 1751-8741
Received on 17th August 2017
Revised 14th December 2017
Accepted on 24th January 2018
doi: 10.1049/iet-nbt.2017.0188
www.ietdl.org

Mohaddeseh Mikani[1], Homa Torabizadeh[1] ✉, Reza Rahmanian[2]

[1]*Department of Food Science & Technology, Iranian Research Organization for Science and Technology (IROST), Tehran, Postal Code: 33853, Iran*

[2]*Young Researchers and Elite Club, North Tehran Branch, Islamic Azad University, Tehran, 32454, Iran*

✉ *E-mail: htoraby@alumni.ut.ac.ir*

Abstract: Magnetic nanoparticles (NPs) were functionalised with soy protein isolate (SPI) and bovine serum albumin (BSA) for inulinase immobilisation. The results revealed the nanomagnetite size of about 50 nm with a polydispersity index (PDI) of 0.242. The average size of the SPI NPs prepared by using acetone was 80–90 nm (PDI, 0.277), and SPI–BSA NPs was 80–90 nm (PDI, 0.233), and their zeta potential was around −34 mV. The mean diameter of fabricated Fe_3O_4@SPI–BSA NPs was <120 nm (PDI, 0.187). Inulinase was covalently immobilised successfully through glutaraldehyde on Fe_3O_4@SPI–BSA NPs with 80% enzyme loading. Fourier transform infrared spectra, field emission scanning electron microscopy, and transmission electron microscopy images provided sufficient proof for enzyme immobilisation on the NPs. The immobilised inulinase showed maximal activity at 45°C, which was 5°C higher than the optimum temperature of the free enzyme. Also, the optimum pH of the immobilised enzyme was shifted from 6 to 5.5. Thermal stability of the enzyme was considerably increased to about 43% at 75°C, and K_m value was reduced to 25.4% after immobilisation. The half-life of the enzyme increased about 5.13-fold at 75°C as compared with the free form. Immobilised inulinase retained over 80% of its activity after ten cycles.

1 Introduction

Nanobiotechnology has gained increasing interest in recent years because of its wide range of applications, including enzyme immobilisation. Nanoparticles (NPs) vary commonly in size between 10 and 1000 nm [1, 2]. Enzyme immobilisation by using nanostructures enhances the functional surface area for enzyme loading, reduces diffusion limitations, and raises catalytic efficiency due to the improvement of particle mobility [3, 4]. Native enzymes generally feature insufficient stability against high temperature and pH variations [5, 6]. As a result, there is a great demand for methods to enhance the stability and reusability of the enzyme. Enzyme immobilisation offers many advantages for industrial applications owing to its convenience in control and ease of enzyme separation from the reaction mixture and recycling, reducing product cost and enhancing thermal and pH enzyme stability [7, 8]. An essential requirement for the immobilisation of enzyme is that the carrier should supply a biocompatible and inert environment, i.e. it should not interfere with the enzyme native structure, and thus, its biological activity is well retained [9].

Magnetic NPs (MNPs) are promising candidates, among others, for carrier-bound immobilisation of the enzymes, owing to their unique physical and chemical properties, such as low toxicity, biocompatibility, superparamagnetism, large surface-to-volume ratio, easy separation under external magnetic fields, and above all, their magnetic properties. MNPs with various surface modifications have been used as the carrier for enzyme immobilisation [10–13]. The construction of versatile core–shell MNPs has been recently established by physical or chemical modification of natural biopolymers on the surface of Fe_3O_4 NPs for functionalising of the particles. Among commonly used biopolymers, proteins are considered one of the most substantial materials for functionalising MNPs; their active surface is mostly attributed to the ε-NH_2 group of lysine amino acid residues as well as superior biocompatibility and hydrophilic properties. Magnetic iron oxide NPs have hydrophobic surfaces with a large surface to volume ratio. Thus, in the absence of any surface coating, these particles tend to form aggregates due to hydrophobic interactions, resulting in an increase of particle size. Moreover, protein NP utilisation for nanomagnetite coating enhances the functional surface area of coated Fe_3O_4, and therefore, it increases enzyme loading [14–16]. In this research, inulinase immobilisation was attempted via covalent binding with soy protein isolate (SPI)–bovine serum albumin (BSA) NPs coated on iron oxide NPs. The preparation of Fe_3O_4@SPI–BSA@inulinase NPs have been discussed in detail.

2 Materials and methods

2.1 Chemicals

Inulinase from *Aspergillus niger* was obtained from Sigma-Aldrich, glutaraldehyde (25% v/v in water), sodium potassium tartrate, 3,5-dinitrosalicylic acid (DNS); SPI was purchased from Merck; and BSA was obtained from Fluka (Germany). All other reagents and solvents used were of analytical grade and obtained from Merck and Sigma–Aldrich.

The dynamic light scattering (DLS) method was employed in the liquid phase using a BI-200 SM Goniometer Version 2 (Brookhaven Instrument Corp., Holtsville, NY, USA). The light scattered by the NPs was detected at 173° through dynamic laser scattering. For electrophoretic mobility determination, which is the relation between the NPs' velocity and the electric applied field, size distribution and mean size were calculated. Additionally, zeta potential was measured by the DLS method and was employed for investigating NPs' stability against aggregation. Surface analysis was performed using a low-vacuum Tescan Mira II field emission scanning electron microscope (Czech Republic) after coating the samples with a thin layer of gold by magnetron sputtering. Energy-dispersive X-ray spectrometry (EDX) is an important non-destructive analytical tool, which was mostly applied for the chemical composition. EDX was also designated by field emission scanning electron microscopy (FE-SEM). Magnetic SPI–BSA NPs size and morphology were measured by transmission electron microscopy (TEM, Philips CM 10 HT-100 kV, Philips Electron Optics, Eindhoven, Netherlands). TEM was performed at 100 kV electron beam accelerating voltage and was equipped with a CCD camera. One drop of the sample solution was deposited onto a

copper grid, and the excess of the droplet was blotted off the grids with filter paper; then, the sample was dried under 25 ± 1 °C. For evaluation of absorbance intensity, a spectrophotometer (Perkin Elmer Lambda 25 UV/VIS, United States) was used. Infrared spectra of all formulations were recorded using a Fourier transform infrared (FTIR) spectroscope (FTIR-8300, Shimadzu, Japan). The NPs were lyophilised before FTIR analysis. The spectra were averaged and levelled and their baselines were calibrated with the Spectra Manager software. The nature of Fe_3O_4@SPI–BSA NPs was studied using the FTIR characterisation method between 400 and 4000 cm^{-1} before and after enzyme immobilisation. FTIR spectra of KBr pellets formed from dry powder samples of Fe_3O_4@SPI–BSA NPs precursor were taken. All the expressed values were mean and standard deviation of three replicate experiments.

2.2 MNPs preparation

Nanomagnetite was prepared by co-precipitation technique. The co-precipitation method is the simplest and most efficient chemical procedure to achieve Fe_3O_4 NPs. The key advantage of the co-precipitation method is that a large-scale of NPs can be produced in a relatively short time. MNPs were prepared by mixing ferric and ferrous chloride in deionised water in 2:1 molar ratio. The system pH was adjusted to 9.5 by NaOH. Black particles of iron oxide were precipitated in the solution at room temperature by stirring with a mechanical stirrer (150 rpm) under nitrogen gas conditions. The particles were separated by high-speed centrifugation at 11,357 ***g*** for 20 min, washed with deionised water three times, and dried in hot air oven at 70° C for 10 h [17–20].

2.3 MNPs modification strategy

Naked MNPs are usually unstable in acidic media and undergo leaching, limiting the reusability and reducing the MNPs lifetime. The high surface-to-volume ratio leads to particle aggregation. Some effective protection strategies, such as coating with biopolymers, were employed to overcome these limitations. For the purpose of this research, SPI–BSA were applied as new natural functionalised protein NPs contain high amounts of lysine residues with reactive ε-NH2 groups for coating the MNPs [14–16].

2.4 SPI NPs fabrication

Desolvation technique was employed for preparing the SPI NPs. At first, SPI powder at concentrations of 1.5–4 mg ml^{-1} was dissolved in deionised water, and its pH was adjusted to 9.0 with 0.1 and 1.0 M NaOH solution during stirring. The influence of SPI concentration on the size of prepared NPs was studied using the DLS method. NPs were obtained by dropwise non-solvent addition to SPI aqueous solution under continuous stirring until the solution became turbid. Ethanol or acetone was applied as a desolvating agent, and the size of attained NPs were reduced by ultrasonication (400 Hz, 10 min, 25 ± 5°C). Finally, the resulting SPI NPs were cross-linked with 380 µl of glutaraldehyde (25% v/v in water). Next, 470 µl of Tween-80 was added to block the non-reacted aldehyde functional group and stabilise the preparation. Large aggregates were eliminated by centrifugation at 11,357 ***g*** for 15 min [21–27].

2.5 Preparation of hybrid SPI–BSA NPs

After optimising the SPI concentration, BSA at different values (12.5–100%) was added to SPI NPs simultaneously and non-simultaneously for preparing hybrid protein NPs. In simultaneous addition, BSA powder was added at different concentrations to SPI powder, and then, desolvating agent was applied to prepare hybrid SPI–BSA NPs. The method was the same as preparation of SPI NPs. In contrast, in non-simultaneous addition, SPI and BSA NPs were prepared separately, and then mixed.

2.6 Fe_3O_4@SPI–BSA NPs carrier preparation

First, 0.06 g of SPI–BSA NPs and 400 µl glutaraldehyde were dissolved in 50 ml of 0.1 M phosphate buffer solution at pH 7.0, and 0.1 g of MNPs was added next. After that, the 300 Hz frequency ultrasound technique was applied for hybrid SPI–BSA NPs binding directly onto MNPs for 10 min at room temperature and stored at ambient temperature overnight. Thereafter, the obtained Fe_3O_4@SPI–BSA NPs were isolated centrifugally at 11,357 ***g*** and washed with deionised water to eliminate the unreacted SPI–BSA NPs as much as possible [15, 16].

2.7 Immobilisation of inulinase enzyme on the Fe_3O_4@SPI–BSA NPs

The covalent immobilisation was done by mixing inulinase solution and Fe_3O_4@SPI–BSA NPs, and stirring for 24 h at 4°C. Glutaraldehyde as a cross-linker (25 mg ml^{-1} aqueous solution), for covalent attachment, was applied in 50 mM sodium acetate buffer at pH 5.4 [7, 8, 28, 29].

2.8 UV spectra of MNPs

UV spectra of Fe_3O_4, SPI–BSA MNPs, and immobilised inulinase on Fe_3O_4@ SPI–BSA were carried out by using a UV-VIS spectrophotometer at 200–600 nm wavelengths.

2.9 Enzyme loading

Immobilised enzymes should preserve the structure, function, and biological activity after immobilisation; enzymes should stay tightly bound to the surface of the carrier and not leached during the use of enzyme [14, 15]. NPs provide a large surface area per unit mass for high enzyme loading. The enzyme loading capacity is estimated through the following equation:

$$Q = \frac{(C_1 - C_2)V}{W}, \tag{1}$$

where Q is the value of enzyme loading (mg enzyme per mg support). C_1 is protein concentration in the inulinase solution before immobilisation. C_2 is the protein concentration of the residual free enzyme in the cocktail after immobilisation. V is the total solution volume, and W is the weight of carrier (mg). The protein content of inulinase was determined by using Bradford's method [30–32].

2.10 Inulinase activity assay

Enzyme activity assay for free and immobilised inulinase was carried out by measuring the amount of reducing sugars released from inulin using the DNS method. Inulinase (100 µl) was incubated with 9000 µl of 50 mM sodium acetate buffer at pH 5.5 and 900 µl of 1 M inulin. The assay mixture for inulinase activity was hydrolysed for 60 min in a water bath at 40°C. Next, the reaction was stopped by adding 500 µl of DNS reagent to 500 µL of the hydrolysed mixture and incubating the mixture at 97–98°C for 10 min. Subsequently, it was cooled, and 167 µl of potassium sodium tartrate 40% solution was added. The absorption of samples was estimated at 575 nm in cells with a 1 cm path length against control. The absorbance was related to the concentration of fructose with a standard calibration curve. All experiments were repeated at least thrice to ensure reproducibility. One unit of inulinase activity was defined as the amount of inulinase enzyme that produced 1 µmol fructose per minute under standard assay conditions [33–35].

2.11 Effect of temperature and pH on free and immobilised inulinase activity

The effect of temperature on the activity of free and immobilised enzyme was determined by incubating enzyme in 0.1 M sodium acetate buffer (pH 5.5) without substrate at different temperatures

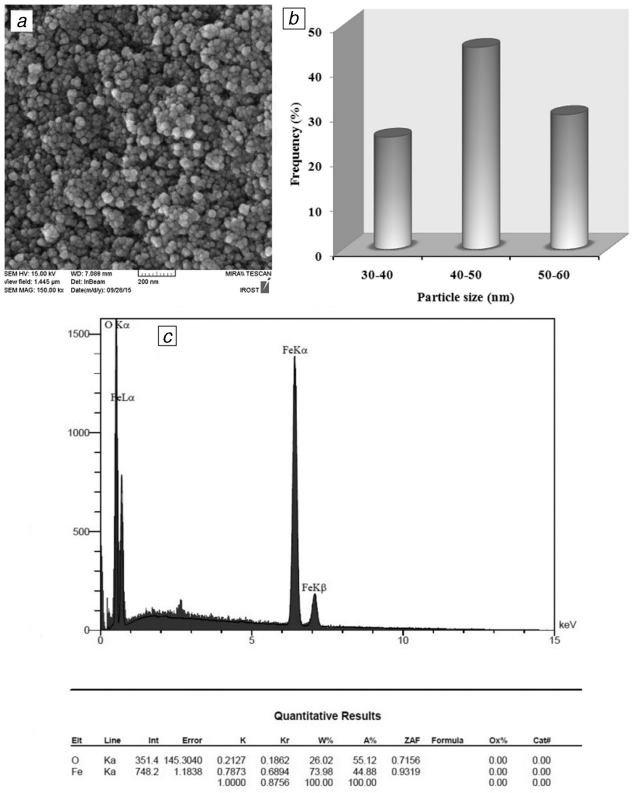

Fig. 1 *Micrograph, size distribution and EDX of nanomagnetite*
(a) *FE-SEM image of nanomagnetite,* ***(b)*** *Nanomagnetite size distribution,* ***(c)*** *EDX for elemental composition of* Fe_3O_4

ranging from 35 to 75°C for 90 min, and then, enzyme activity was determined by the DNS method as described earlier. For determining the effect of pH on enzyme activity, various pH ranges 3–8 (pH 3–5, 0.1 M acetate buffer; pH 6–8, phosphate buffer) at 40°C were performed [36].

2.12 Determination of thermal stability and enzyme half-life

The thermal stability of free and immobilised inulinase and, subsequently, enzyme half-life was estimated in temperature ranging from 35 to 75°C for 90 min hydrolysis. The highest enzyme activity was expressed as 100%, and the relative activity at each temperature was expressed as a percentage of the maximum activity. The inactivation rate constant (k_{in}) was specified by plotting the *Ln* percentage remaining activity against time for each temperature and using (2) subsequently for determination of enzyme half-life [36]

$$t_{1/2} = \ln 2/k_{in}. \quad (2)$$

2.13 Determination of kinetic parameters

Michaelis constant K_m and V_{max} were measured by applying different inulin concentrations (0.25–5 mg ml^{-1}) in sodium acetate buffer (0.1 M, pH 5.5) at 40°C. The Lineweaver–Burk plot was used for specifying kinetic constants of free and immobilised inulinase [28, 37].

2.14 Reusability of immobilised inulinase

Reusability was performed by incubating 100 µl immobilised inulinase with 9000 µl of 50 mM sodium acetate buffer at pH 5.5 and 900 µl inulin solution (1%) and hydrolysing the mixture for 60 min in a water bath at 40°C. Then, enzyme activity was determined by the DNS method.

After each cycle, the enzyme was separated by centrifugation and washed with sodium acetate buffer before re-adding into a fresh reaction mixture for the next step hydrolysis [38].

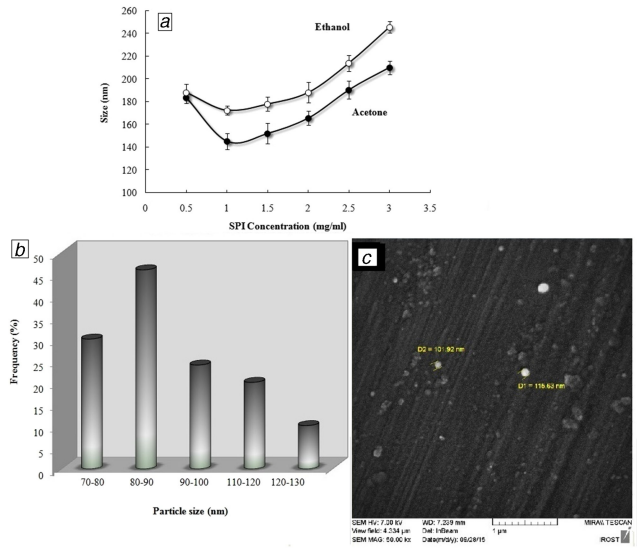

Fig. 2 *Particle size in two solvent system, size distribution and micrograph of SPI*
(a) Effect of SPI concentration on the size of soy protein NPs at two types of desolvating agents based on DLS results, ***(b)*** SPI NPs size distribution based on DLS results, ***(c)*** FE-SEM image of the SPI NPs

3 Results and discussion

3.1 Step-by-step Fe_3O_4@SPI–BSA@inulinase preparation and morphological characterisation study

The morphology and size of the fabricated MNPs were investigated using FE-SEM and DLS methods. The FE-SEM image of the prepared MNPs and size distribution graph are shown in Figs. 1*a* and *b*. The obtained water-based MNPs possessed spheres and irregular spheres with a mean diameter of about 50 nm and a polydispersity index (PDI) of 0.242. The existence of the MNPs was confirmed by means of EDX, which determined the elemental composition of Fe_3O_4 (Fig. 1*c*).

3.2 SPI NPs fabrication at the optimised condition

A comparative study of the effect of SPI concentration on NPs size and distribution for two types of desolvating agents (ethanol and acetone) was performed (Fig. 2*a*).

As shown in Fig. 2*a*, by increasing the initial SPI concentration from 1.5 to 4 mg ml^{-1}, the particle size is enhanced. This difference might be attributed to the fact that higher protein concentration favoured the collision and aggregation of protein molecules [24]. The concentration of SPI in the initial solution is a significant factor in the process of particle formation, which might be explained by considering the classical theory of nucleation. The resultant optimum SPI concentration was 2 mg ml^{-1}. The size range of SPI NPs prepared by using acetone was 80–130 nm with PDI of 0.277 (Fig. 2*b*), lower than ethanol for all SPI concentrations. Organic solvents such as acetone and ethanol have the ability to promote nucleation and precipitation of SPI molecules to aggregate, since SPI is insoluble in them, and the aggregation process results spontaneously in NPs [23, 24, 26, 27].

The FE-SEM images of lyophilised NPs confirmed DLS results, but the effective diameter of the particles using DLS measurement was a little bigger than results from FE-SEM image (Fig. 2*c*). This difference can possibly be attributed to the shrinkage caused by the cast-drying process as well as the vacuum environment in the FE-SEM image [24]. It was obvious that most of the resulting SPI NP morphologies were semi-spherical.

3.3 Hybrid SPI–BSA NP fabrication

In the next step, the effect of SPI—BSA ratios versus the size of produced SPI–BSA NPs was analysed. The results are shown in Fig. 3. The SPI–BSA NPs' size decreased from 12.5 to 37.5% BSA and then increased from 37.5 to 100% BSA concentration in a

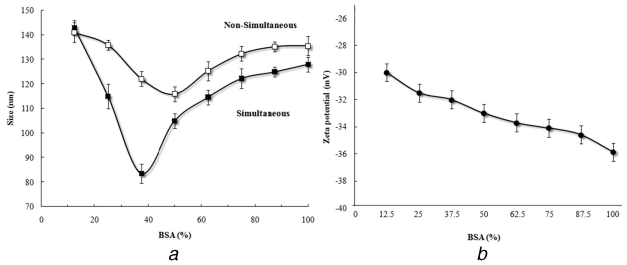

Fig. 3 *The effect of BSA concentration on the size and zeta-potential of SPI-BSA*

(a) Effect of BSA concentration at simultaneous and non-simultaneous process on the size of SPI–BSA NPs based on DLS results, ***(b)*** Effect of BSA concentration on zeta potential of SPI–BSA NPs

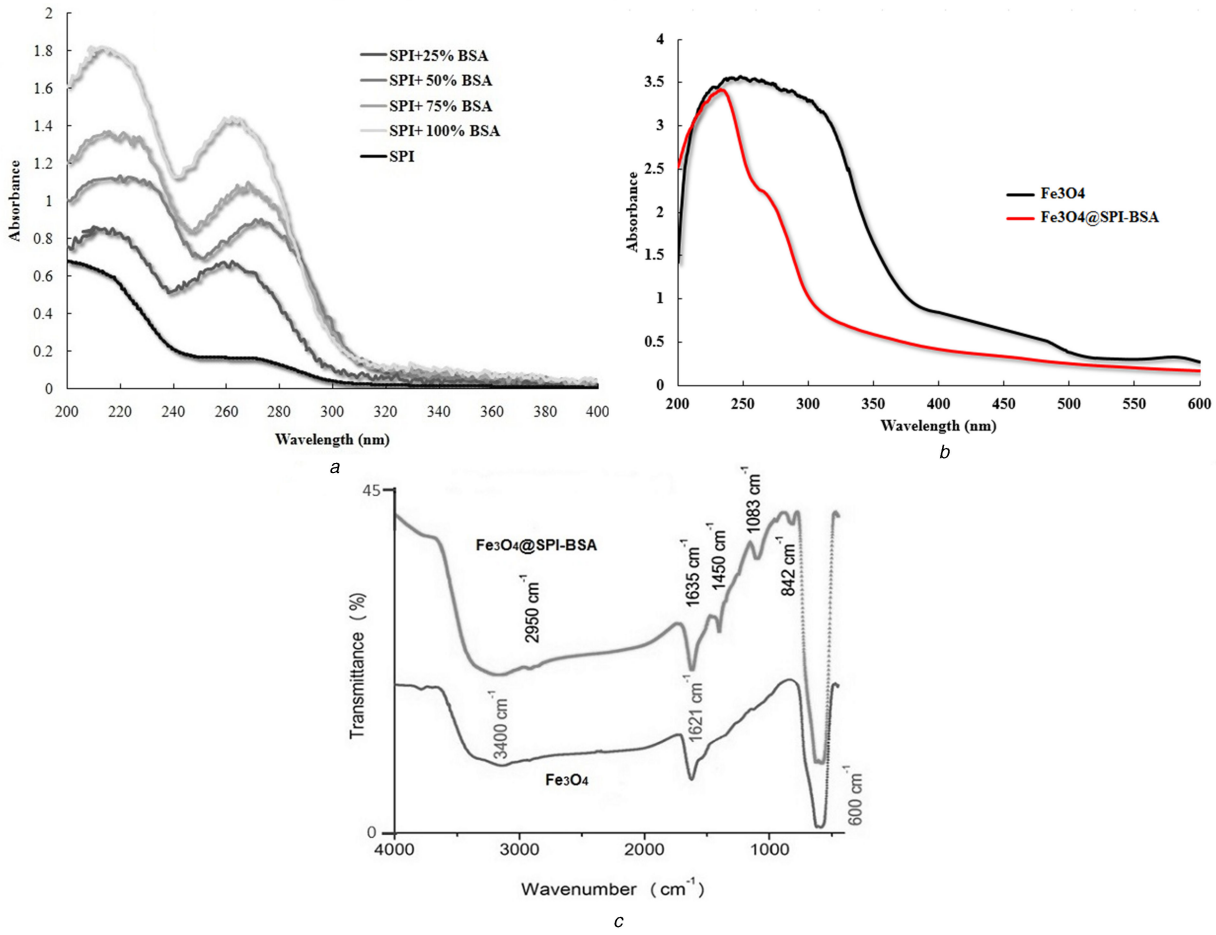

Fig. 4 *UV-Vis and FTIR spectra of SPI–BSA and Fe_3O_4@SPI–BSA NPs*

(a) UV-Vis spectra of SPI–BSA NPs at different BSA concentrations, ***(b)*** Comparative spectrum of Fe_3O_4 and Fe_3O_4@SPI–BSA NPs, ***(c)*** FTIR spectrum of Fe_3O_4 nanostructure before and after coating by SPI–BSA NPs

simultaneous procedure. Conversely, in a non-simultaneous procedure, the SPI–BSA NP's size decreased from 12.5 to 50% BSA and increased 50–100% BSA concentration, respectively (Fig. 3*a*). In the simultaneous process, the size range of SPI–BSA NPs was lower for all BSA concentrations compared with the non-simultaneous process.

The effect of BSA concentration in hybrid SPI–BSA NPs on zeta potential is shown in Fig. 3*b*. As indicated, by adding BSA to SPI, zeta potential increases proportionately with increasing BSA. These changes can be attributed to the negative surface charge of BSA molecules, which results in a gradual increase in electrostatic repulsion between NPs and a decrease in aggregation of particles. NPs with a zeta potential above ±30 mV have been shown to be stable in suspension, as the surface charge prevents the aggregation of particles [39, 40]. Moreover, the PDI for SPI–BSA NPs was 0.233, lower than the resultant PDI for SPI (0.277), which indicates that BSA enhances the hydrophilicity of SPI–BSA NPs. Eventually, according to the results obtained by determining the hybrid SPI-BSA NPs size and zeta potential, the optimum amount for adding BSA to SPI in a simultaneous process was selected to be 37.5%.

3.4 UV-Vis and FTIR spectra of fabricated NPs

SPI NPs possessed two main λ_{max} in the UV region; one between 215–230 nm, where peptide bonds absorbed, and second at 280 nm due to the light absorption by aromatic amino acids (Fig. 4*a*) [41, 42]. The results revealed that after addition of 0.25–1 mg ml^{-1} BSA to 1 mg ml^{-1} SPI during the NP preparation, peptide bonds and aromatic amino acids are reinforced, and the protein structure is preserved during NP preparation. Moreover, UV spectra of Fe_3O_4 and Fe_3O_4@SPI–BSA implied that, after Fe_3O_4 functionalisation, two new peaks are formed one at 235 nm and another at 265–275 nm, which can be attributed to the binding of SPI and BSA to MNPs (Fig. 4*b*).

As shown in Fig. 4*c*, the spectrum before enzyme immobilisation indicated Fe–O stretching vibration at 600 cm^{-1},

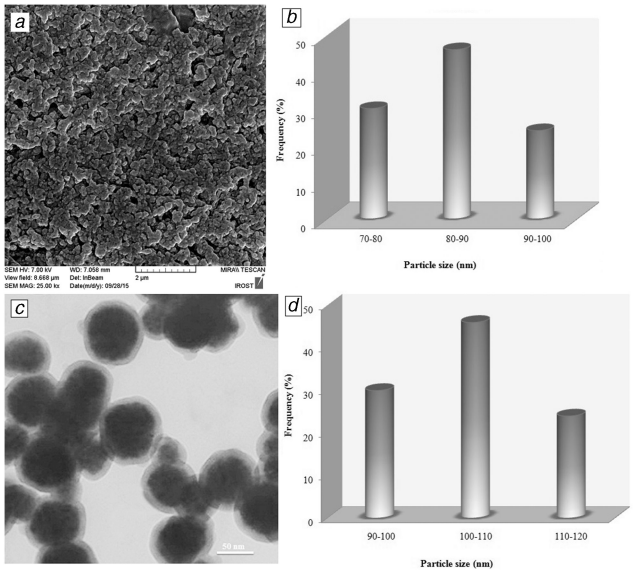

Fig. 5 *Morphology and size of Fe_3O_4@SPI–BSA NPs by FE-SEM, TEM, and DLS method*

(a) SPI–BSA NPs morphology, ***(b)*** Size distribution of SPI–BSA NPs, ***(c)*** TEM image of immobilised inulinase on Fe_3O_4@SPI–BSA NPs, ***(d)*** Particle size distribution of inulinase on Fe_3O_4@SPI–BSA NPs

the adsorbed water molecules stretching at 1621 cm^{-1} and an intense OH band around 3400 cm^{-1}. The OH band corresponded to the stretching vibrations of Fe–OH groups attached on the Fe_3O_4 surface and can be pointed to the remaining water that was not omitted from the nanomagnetite surface. The SPI peaks at 1450, 2950, and 1635 cm^{-1} were attributed to the stretching vibration mode of C=O, N–H, COO bonds, respectively. The significant peak of BSA at 1637 cm^{-1} corresponded to the vibrations of the backbone C=O, belonging to the vibration of amide groups in the FTIR spectrum overlapped by the Fe_3O_4 peak. After enzyme immobilisation, the peaks at 1253, 1522, and 2950 cm^{-1} attributed to the stretching vibration of C–O–C, bending vibration of N–H, and stretching vibration of C–H, respectively [24, 41, 43, 44].

3.5 Fe_3O_4@SPI–BSA@inulinase characteristics

The morphology and size of hybrid SPI–BSA NPs were investigated by the FE-SEM and DLS method. The SPI–BSA NPs possessed spherical morphology (Fig. 5*a*), and DLS results revealed SPI–BSA NPs were found to be in the range of 70–100 nm and mean size of about 85 nm (Fig. 5*b*).

The mean diameter of Fe_3O_4@SPI–BSA NPs was <120 nm (PDI, 0.187), which was bigger than the naked nanomagnetite. The size difference demonstrated that the SPI–BSA NPs were coated on MNPs successfully. The resultant TEM image shows that after coating of a magnetic core by a shell of SPI–BSA, the resultant Fe_3O_4@SPI–BSA NPs were still spherical (Fig. 5*c*) with a size increase to about 90–120 nm. The particle-size distribution graph is shown in Fig. 5*d*. Finally, the TEM image indicated the successful immobilisation of inulinase on Fe_3O_4@SPI–BSA NPs, which retained its activity and natural structure required for improving inulin hydrolysis in industrial media.

3.6 Enzyme loading

The results of this study indicated that the enzyme loading under the described immobilisation conditions were nearly 80%.

3.7 Inulinase activity assay

The outcomes of this work show that the optimal activity of free inulinase results after 3 min of reaction at temperatures between 35–40°C. However, in the case of the immobilised enzyme, this time is altered to 5 min (Fig. 6*a*). In this case, enzyme activity reduces by about 3.7% after immobilisation, but fructose production (mg ml^{-1}) is enhanced by 49.6% after 60 min (Fig. 6*b*). Thus, 80% of the enzyme that was loaded as immobilised inulinase was active.

3.8 Effect of temperature and pH on free and immobilised inulinase activity

The optimum temperature of the immobilised enzyme, as compared with the free state, was found to have shifted from 40°C to 45°C (Fig. 6*c*). It was 5°C higher than that of free enzyme. This shift of the enzyme's optimum temperature after immobilisation could be attributed to the formation of a molecular cage around the enzyme molecule that protected the enzyme's molecules from the bulk temperature [34, 35].

The results clearly indicate that at 45°C, the relative activity of the immobilised enzyme was considerably increased compared with other temperatures studied (35, 55, 65, and 75°C).

Lower optimum pH is useful for the preparation of high fructose syrup because it avoids unwanted colour formation [35, 45]. The highest activity of inulinase was observed at pH 6.0, whereas the optimum pH of the immobilised enzyme was shifted (Fig. 6*d*). This shift occurs in the direction of acidic pH (pH 5.5). This pH shift appears partially because there exist a micro-environmental difference such as the surface charge of the carrier material [35].

As shown in Fig. 6, free and immobilised enzymes were quite stable in the pH range from 4.5 to 7.5, and pH stability was basically enhanced after immobilisation.

3.9 Determination of enzyme half-life

The results indicated an improved half-life of the immobilised enzyme compared with the free form. Obviously, $t_{1/2}$ values reduced with an increase in the incubation temperature [36, 38]. However, $t_{1/2}$ values of immobilised enzyme were significantly higher than that of the free form at the chosen incubation temperature. As a result, the immobilised inulinase was more stable than the free enzyme (Table 1).

3.10 Determination of kinetic parameters

The kinetic constants of native and immobilised inulinase were estimated using the Lineweaver–Burk plot. The calculated values are shown in Table 2.

After immobilisation, the K_m value decreased, which demonstrates only a small amount of substrate is needed to saturate the enzyme. This indicates a high affinity for the substrate. Such a small reduction in both K_m and V_{max} values after immobilisation is common.

3.11 Reusability study

The primary advantage of immobilisation of enzyme is the easy separation and reusability [38]. Fig. 7 shows that the immobilised inulinase retained over 80% of its activity after 10 cycles. It was observed that there was no significant loss in activity up to four cycles, but afterwards, the activity started to reduce.

4 Conclusion

SPI–BSA functionalised MNPs were synthesised by the co-precipitation method using acetone as the desolvating agent. SPI concentration was optimised; the simultaneous addition of BSA NPs resulted in the formation of SPI–BSA NPs with 83.5 nm size and − 34 mV zeta potential, which revealed good stability. Inulinase immobilisation on Fe_3O_4@SPI–BSA NPs was successfully accomplished with 80% enzyme loading, and fructose production was enhanced by 49.6% after 60 min. The thermal stability of the immobilised inulinase was improved by 50–70°C also, and the optimal pH of the enzyme became more acidic than the free enzyme. The K_m value (Michaelis constant) of

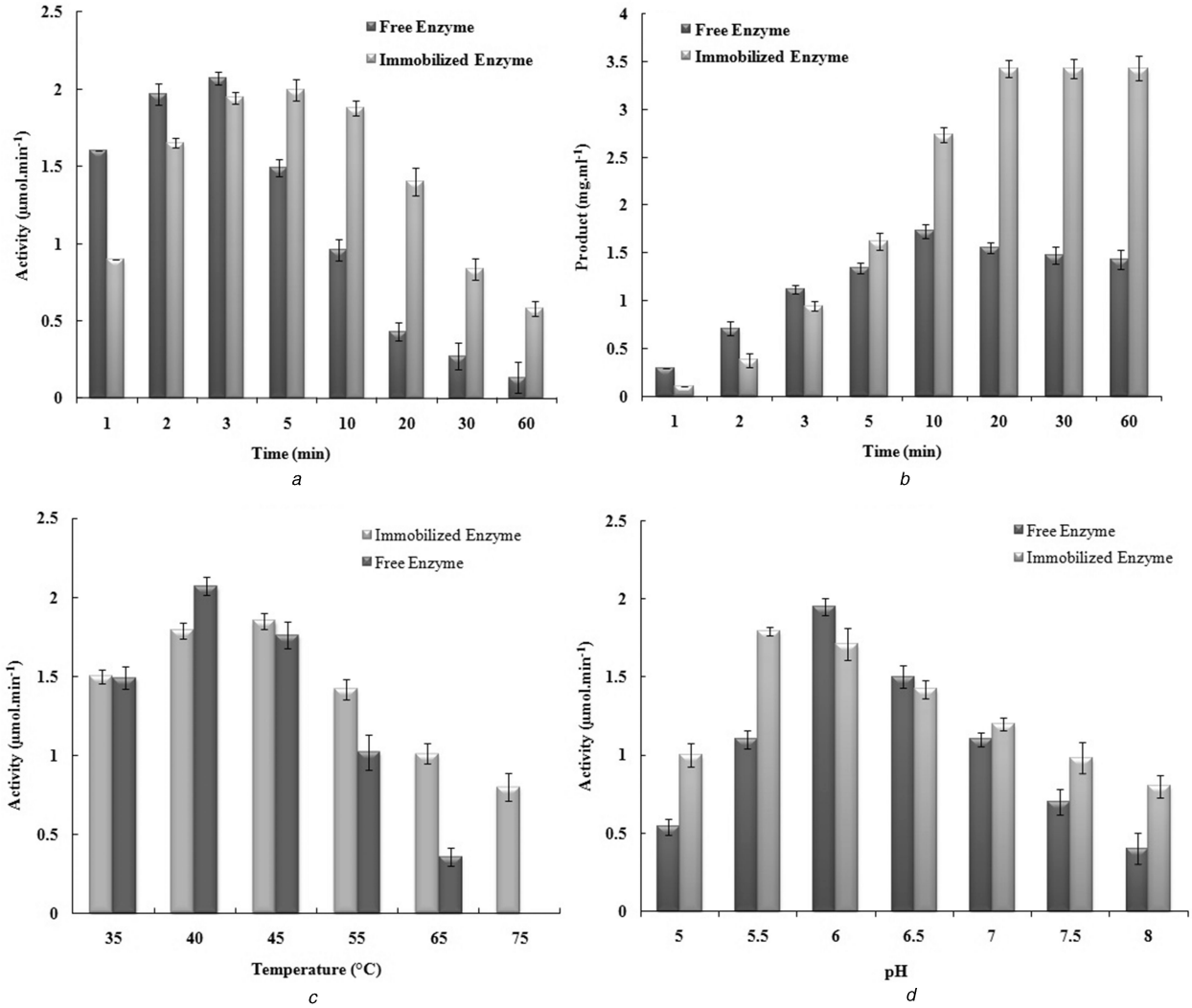

Fig. 6 *Enzyme activity and hydrolysis profile, effect of temperature and pH on enzyme activity of free and immobilised inulinase*
(a) Comparison of enzyme activity of free and immobilised inulinase, ***(b)*** Hydrolysis profile of free and immobilised inulinase, ***(c)*** Effect of temperature and pH on enzyme activity

Table 1 Half-life of the free and immobilised enzyme at three different temperatures

	Half-life, min		
	55°C	65°C	75°C
free enzyme	182	63	30
immobilised enzyme	495	407	154

Table 2 Michaelis–Menten constant (K_m) and V_{max} of free and immobilised inulinase

	K_m, mg ml^{-1}	V_{max}, μmol min^{-1}
free enzyme	2.72	0.829
immobilised enzyme	2.03	0.624

immobilised inulinase implied 25.4% reduction compared with the free enzyme, which indicates a high affinity for the substrate.

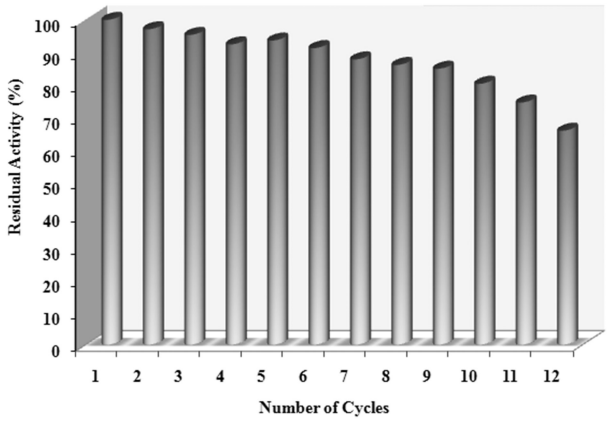

Fig. 7 *Effect of the enzyme reuses on the activity of immobilised inulinase during inulin hydrolysis at pH 5.5 and 40°C for 60 min; each treatment was performed in triplicate*

5 Acknowledgments

The financial support provided by the Iranian Research Organisation for Science and Technology (IROST) and Iran Nanotechnology Initiative Council (INIC) is greatly acknowledged.

6 References

[1] Couvreur, P., Gref, R., Andrieux, K., *et al.*: 'Nanotechnologies for drug delivery: application to cancer and autoimmune diseases', *Prog. Solid State Chem.*, 2006, **34**, (2–4), pp. 231–235

[2] Kumaresh, S., Aminabhavi, T.M., Kulkarni, A.R., *et al.*: 'Biodegradable polymeric nanoparticles as drug delivery devices', *J. Control. Release*, 2001, **70**, (1–2), pp. 1–20

[3] Xie, T., Wang, A.M., Huang, L.F., *et al.*: 'Recent advance in the support and technology used in enzyme immobilization', *Afr. J. Biotechnol.*, 2009, **8**, (19), pp. 4724–4733

[4] Jia, H., Zhu, G., Wang, P.: 'Catalytic behaviors of enzymes attached to nanoparticles: the effect of particle mobility', *Biotechnol. Bioeng.*, 2003, **84**, (4), pp. 406–414

[5] Datta, S., Christena, L.R., Rani, Y., *et al.*: 'Enzyme immobilization: an overview on techniques and support materials', *Biotechnology*, 2012, **3**, (1), pp. 1–9

[6] Subramanian, A., Kennel, S.J., Oden, P.I., *et al.*: 'Comparison of techniques for enzyme immobilization on silicon supports – effect of cross-linker chain length on enzyme activity', *Enzyme Microb. Technol.*, 1999, **24**, (1), pp. 26–34

[7] Torabizadeh, H., Tavakoli, M., Safari, M.: 'Immobilization of thermostable α-amylase from *Bacillus licheniformis* by cross-linked enzyme aggregates method using calcium and sodium ions as additives', *J. Mol. Catal. B, Enzym.*, 2014, **108**, (1), pp. 13–20

[8] Richetti, A., Munaretto, C.B., Lerin, L.A., *et al.*: 'Immobilization of inulinase from *Kluyveromyces marxianus* NRRL Y-7571 using modified sodium alginate beads', *Bioprocess Biosys. Eng.*, 2012, **35**, (3), pp. 383–388

[9] Mitchell, D.T., Lee, S.B., Trofin, L., *et al.*: 'Smart nanotubes for bioseparations and biocatalysis', *J. Am. Chem. Soc.*, 2002, **124**, (40), pp. 11864–11865

[10] Reddy, L., Arias, J., Nicolas, J., *et al.*: 'Magnetic nanoparticles: design and characterization, toxicity and biocompatibility, pharmaceutical and biomedical application', *Chem. Rev.*, 2012, **112**, (11), pp. 5818–5878

[11] Couto, G., Klein, J., Schreiner, W., *et al.*: 'Nickel nanoparticles obtained by a modified polyol process: synthesis, characterization, and magnetic properties', *J. Colloid Interface Sci.*, 2007, **311**, (2), pp. 461–468

[12] Sun, C., Lee, J., Zhang, M.: 'Magnetic nanoparticles in MR imaging and drug delivery', *Adv. Drug Deliv. Rev.*, 2008, **60**, (11), pp. 1252–1265

[13] Liang, X., Shi, H., Jia, X., *et al.*: 'Dispersibility, shape and magnetic properties of nano-Fe_3O_4 particles', *Mater. Sci. Appl.*, 2011, **2**, (11), pp. 1644–1653

[14] Gupta, A., Gupta, M.: 'Synthesis and surface engineering of iron oxide nanoparticles for biomedical applications', *Biomaterials*, 2005, **26**, (18), pp. 3995–4021

[15] Mikhaylova, M., Kim, D.K., Catherine, C., *et al.*: 'BSA immobilization on amine-functionalized superparamagnetic iron oxide nanoparticles', *Chem. Mater.*, 2004, **16**, (12), pp. 2344–2354

[16] Zhanfeng, L., Linhui, Q., Shuangling, Z., *et al.*: 'Synthesis and characterization of monodisperse magnetic Fe_3O_4@BSA core–shell nanoparticles', *Colloids Surf. A*, 2013, **436**, (1), pp. 1145–1151

[17] Nedkov, I., Merodiiska, T., Slavov, L., *et al.*: 'Surface oxidation, size and shape of nano-sized magnetite obtained by co-precipitation', *J. Magn. Magn. Mater.*, 2006, **300**, (2), pp. 358–367

[18] Itoh, H., Sugimoto, T.: 'Systematic control of size, shape, structure, and magnetic properties of uniform magnetite and maghemite particles', *J. Colloid Interface Sci.*, 2003, **265**, (2), pp. 283–295

[19] Mascolo, M.C., Pei, Y., Ring, T.A.: 'Room temperature co-precipitation synthesis of magnetite nanoparticles in a large pH window with different bases', *Materials*, 2013, **6**, (12), pp. 5549–5567

[20] Kandpal, N.D., Sah, S., Loshali, R., *et al.*: 'Coprecipitation method of characterization of iron oxide nanoparticles', *J. Sci. Ind. Res.*, 2014, **73**, (2), pp. 87–90

[21] Lohcharoenkal, W., Wang, L., Chen, Y.C., *et al.*: 'Protein nanoparticles as drug delivery carriers for cancer therapy', *J. Biomed. Biotechnol.*, 2014, **2014**, (1), pp. 1–15

[22] Joye, I.J., Nelis, V.A., McClements, D.J.: 'Gliadin-based nanoparticles: fabrication and stability of food-grade colloidal delivery systems', *Food Hydrocoll.*, 2014, **43**, (1), pp. 236–242

[23] Weber, C., Coester, C., Kreuter, J., *et al.*: 'Desolvation process and surface characterization of protein nanoparticles', *Int. J. Pharm.*, 2000, **194**, (1), pp. 91–102

[24] Teng, Z., Luo, Y., Wang, Q.: 'Nanoparticles synthesized from soy protein: preparation, characterization, and application for nutraceutical encapsulation', *J. Agric. Food Chem.*, 2012, **60**, (10), pp. 2712–2720

[25] Krishna, S.A., Amareshwar, P., Chakravarty, P.: 'Different techniques used for the preparation of nanoparticles using natural polymers and their application', *J. Pharm. Pharm. Sci.*, 2011, **3**, (2), pp. 45–50

[26] Jun, J.Y., Nguyen, H.H., Paik, S.Y.R., *et al.*: 'Preparation of size-controlled bovine serum albumin (BSA) nanoparticles by a modified desolvation method', *Food Chem.*, 2011, **127**, (4), pp. 1892–1898

[27] Galisteo-González, F., Molina-Bolívar, J.A.: 'Systematic study on the preparation of BSA nanoparticles', *Colloids Surf. B.*, 2014, **123**, (1), pp. 286–292

[28] Elnashar, M.M., Danial, E.N., Awad, G.E.: 'Novel carrier of grafted alginate for covalent immobilization of inulinase', *Ind. Eng. Chem. Res.*, 2009, **48**, (22), pp. 9781–9785

[29] Sheldon, R.A.: 'Enzyme immobilization: the quest for optimum performance', *Adv. Synth. Catal.*, 2007, **349**, (8–9), pp. 1289–1307

[30] Torabizadeh, H., Habibi-Rezaei, M., Safari, M., *et al.*: 'Semi-rational chemical modification of endoinulinase by pyridoxal 5′-phosphate and ascorbic acid', *J. Mol. Catal. B: Enzym.*, 2010, **62**, (1), pp. 257–264

[31] Bradford, M.M.: 'A rapid and sensitive method for the quantitation of microgram quantities of protein utilizing the principle of protein-dye binding', *Anal. Biochem.*, 1976, **72**, (1), pp. 248–254

[32] Mohamed, T.M., El-Souod, S.M., Ali, E.M., *et al.*: 'Immobilization and characterization of inulinase from *Ulocladium atrumon* nonwoven fabrics', *J. Biosci.*, 2014, **39**, (1), pp. 785–793

[33] Missau, J., Scheid, A.J., Foletto, E.L., *et al.*: 'Immobilization of commercial inulinase on alginate–chitosan beads', *Sustain. chem. Process.*, 2014, **2**, (1), pp. 2–13

[34] Catana, R., Ferreira, B.S., Cabral, J.M., *et al.*: 'Immobilization of inulinase for sucrose hydrolysis', *Food Chem.*, 2005, **91**, (1), pp. 517–520

[35] Santos, A.M.P., Oliveira, M.G., Maugeri, F.: 'Modelling thermal stability and activity of free and immobilized enzymes as a novel tool for enzyme reactor design', *Bioresour. Technol.*, 2007, **98**, (16), pp. 3142–3148

[36] Ghada, E.A., Hala, R., Wehaid, A.A., *et al.*: 'A novel alginate–CMC gel beads for efficient covalent inulinase immobilization', *Colloid Polym. Sci.*, 2017, **295**, (3), pp. 495–506

[37] Singh, R.S., Singh, R.P., Kennedy, J.F.: 'Immobilization of yeast inulinase on chitosan beads for the hydrolysis of inulin in a batch system', *Int. J. Biol. Macromol.*, 2017, **95**, (1), pp. 87–93

[38] Nguyen, Q.D., Rezessy, J.M., Czukor, B., *et al.*: 'Continuous production of oligofructose syrup from *Jerusalem artichoke* juice by immobilized endo-inulinase', *Process Biochem.*, 2011, **46**, (1), pp. 298–303

[39] Mehravar, R., Jahanshahi, M., Saghtoleslami, N.: 'Fabrication and evaluation of human serum albumin (HSA) nanoparticles for drug delivery application', *Int. J. Nanosci.*, 2009, **8**, (3), pp. 319–322

[40] Jahanshahi, M., Najafpour, G.D., Rahimnejad, M.: 'Applying the Taguchi method for optimized fabrication of bovine serum albumin (BSA) nanoparticles as drug delivery vehicles', *Afr. J. Biotechnol.*, 2008, **7**, (4), pp. 362–367

[41] Skoog, D.A., Holler, F.J., Crontch, S.R.: '*Principles of instrumental analysis*' (Thomson Brooks/Cole., Canada, 2007, 6th edn.), pp. 237–250

[42] Singh, P., Gill, P.K.: 'Production of inulinases: recent advances', *Biotechnol.*, 2006, **44**, (2), pp. 151–162

[43] Zhang, J., Liang, L., Tian, Z., *et al.*: 'Preparation and in vitro evaluation of calcium-induced soy protein isolate nanoparticles and their formation mechanism study', *Food Chem.*, 2012, **133**, (2), pp. 390–399

[44] Sundar, S., Kundu, J., Kundu, S.C.: 'Biopolymeric nanoparticles', *Sci. Tech. Adv. Mater.*, 2010, **11**, (1), pp. 1–13

[45] Yewale, T., Singhal, R.S., Vaidya, A.A.: 'Immobilization of inulinase from *Aspergillus niger* NCIM 945 on chitosan and its application in continuous inulin hydrolysis', *Biocatal. Agric. Biotechnol.*, 2013, **2**, (1), pp. 96–101